Bubble-induced turbulence suppression in Langmuir circulation

Johannes Gemmrich[1]

Received 13 March 2012; revised 14 April 2012; accepted 16 April 2012; published 17 May 2012.

[1] Dissipation rates ϵ of turbulent kinetic energy and air bubble characteristics were observed within the wave-enhanced near-surface layer in the open ocean. During a period of well developed Langmuir circulation, short periods of increased air fraction and peak bubble radii <150 μm at 2.5m, indicative of the instrumentation package drifting through convergence zones, coincide with significantly reduced dissipation rates. The rate of turbulence suppression correlates well with the buoyancy frequency inferred from the vertical gradient of air fraction. The Ozmidov scale and turbulent time scales associated with the bubble induced stratification are of O(0.5m) and O(20–60s), respectively. These stratification characteristics are consistent with the suppression of energy containing eddies close to the surface, which in turn results in reduced turbulent dissipation rates. Dissipation rates are observed to decay with depth following a power law $\epsilon \propto z^n$, and $n = -1$, consistent with the theoretical value for constant stress layer scaling, is found within convergence zones, but $n \approx -3$ outside. **Citation:** Gemmrich, J. (2012), Bubble-induced turbulence suppression in Langmuir circulation, *Geophys. Res. Lett.*, *39*, L10604, doi:10.1029/2012GL051691.

1. Introduction

[2] The air to sea transfer of momentum is largely supported by surface waves. When the waves break turbulent kinetic energy is injected into the surface layer and dissipation rates ε briefly exceed that predicted by constant stress layer scaling $\varepsilon_{wl} = u_*^3/\kappa z$ by up to 3 orders of magnitude [*Gemmrich and Farmer*, 2004], where z, u_* and $\kappa = 0.4$ are depth, friction velocity in the water, and the von Karman constant, respectively. The vertical penetration of the breaking wave induced turbulence is comparable to the significant wave height H_s. Breaking waves also generate plumes of air bubbles. Coherent structures such as Langmuir circulation (hereafter LC) organize the bubbles into elongated bands approximately aligned with the wind, where they are advected downward to more than 15m [e.g., *Thorpe*, 1992; *Farmer and Li*, 1995]. It is now recognized that LC exist on a wide range of horizontal scales and therefore is commonly labeled Langmuir turbulence [e.g., *McWilliams et al.*, 1997; *Teixeira and Belcher*, 2010]. LC plays an important role in upper ocean mixing, and LES models require the inclusion of LC to correctly model the deepening of the mixed layer [*Kukulka et al.*, 2009]. Whereas there are sufficient observations of the structured bubble plumes within LC, the question arises whether LC organizes turbulence in a similar way.

[3] Observation with an autonomous underwater vehicle showed roughly 50% dissipation enhancement within LC convergence zones at depth > $2H_s$ [*Thorpe et al.*, 2003]. Measurements with a neutrally buoyant float showed the mean turbulent kinetic energy in the mixed layer is about twice as high in the presence of LC compared to a pure shear flow [*D'Asaro*, 2001], a result that is well reproduced by LES models of Langmuir turbulence [*Li et al.*, 2005]. However, there are no turbulence observations within the wave-enhanced layer in LC, or model results that include potential buoyancy effects due to bubble stratification. Recent observations showed a reduction of near-surface turbulence due to thermal stratification [*Vagle et al.*, 2012]. Here I argue that turbulence may also be suppressed by stratification associated with strong vertical gradients in air fraction, an effect not considered in upper ocean models, so far.

2. Observations

[4] Observations of the turbulent velocity and bubble field were taken October 10, 2000, 10:00–12:30 UTC as part of the FAIRS (Fluxes, Air-sea Interaction and Remote Sensing) experiment aboard R/P FLIP in the open ocean at wind speed $u_{10} = 14\mathrm{m\ s}^{-1}$, unlimited fetch and nearly fully developed waves with $H_s = 3$m. High resolution vertical velocity profiles 1–1.7m below the free surface were obtained with a pulse-to-pulse coherent acoustic Doppler sonar (DopBeam) supported from a tethered float. Dissipation estimates are calculated according to the inertial sub range method [*Gemmrich and Farmer*, 2004] at 3 different depths, based on wave number spectra from 3 equal length subsections of the velocity profile. Here we are interested in more persistent turbulence features of LC, and dissipation rates are obtained from the inertial sub range of an average spectrum from 200 individual velocity wave-number spectra, yielding a 10 s sampling rate for the dissipation time series. The bubble field was monitored with two acoustic resonators at 0.85m and 2.5m depth, and the bubble size distribution and air fraction of bubbles in the range 20–400 μm were obtained. In addition, eight sidescan sonars mounted on the hull of FLIP monitored the larger scale bubble plumes up to a range of 250m. R/P FLIP drifted freely, and the side-scanning sonar images show the advection of LC relative to R/P FLIP. Thus, the tethered sensor float continuously traversed individual LC convergence zones. However, the float was not aligned with the sonar beams and therefore the exact phase of the LC-float encounter cannot be determined from the sonar images.

2.1. Individual LC Convergence

[5] Occurrences of the instrument package drifting across a LC convergence are best identified by the presence of

[1]Department of Physics and Astronomy, University of Victoria, Victoria, British Columbia, Canada.

Corresponding author: J. R. Gemmrich, Department of Physics and Astronomy, University of Victoria, PO Box 3055, Victoria, BC V8W 3P6, Canada. (gemmrich@uvic.ca)

0094-8276/12/2012GL051691

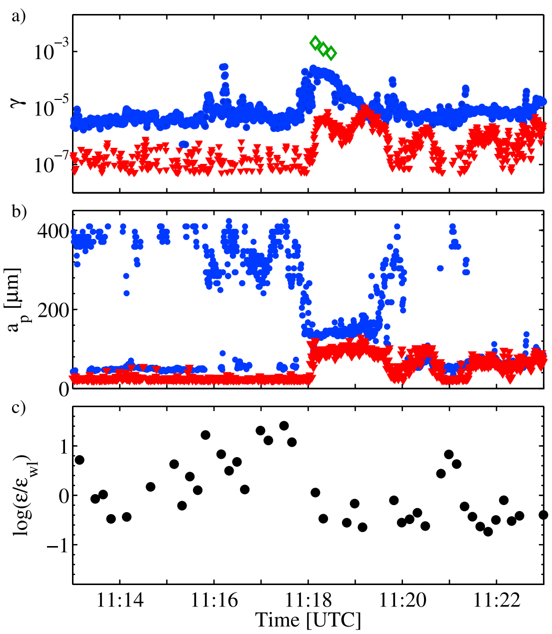

Figure 1. Float measurements related to the instrument traversing a Langmuir convergence zone at t = 11:18. (a) Air fraction at 2.5m (red triangles), 0.85m (blue dots) and 0.05m (estimated, green diamonds). (b) Radius of peak of bubble size distribution at 2.5m (red) and 0.85m (blue), (c) normalized average dissipation at 0.8m to 1.5m.

bubbles at the lower resonator (Figure 1a). Typically, the period needed for the float to cross a convergence zone is about 2–3 minutes, after which the air fraction drops again. Between convergences, air fraction γ at 2.6m is less than the detection level of the resonators ($O(10^{-7})$), but rises to $\gamma > 10^{-6}$ within the convergence. Mean air fraction at the shallow resonator (0.85m) is $\approx 5 \times 10^{-6}$. For brief periods within breaking waves γ(0.85m) surpasses the resonator's upper measurement limit ($O(10^{-4})$). Within convergences this limit is usually not reached unless it coincides with an actively breaking event, in which case the data are excluded from the subsequent analysis. Bubble plumes generated by wave breaking contain a wide range of bubble sizes with the largest radii being up to O (1 mm) [*Deane and Stokes*, 2002]. Larger bubbles rise faster to the surface than smaller ones, leaving predominately smaller bubbles accumulated within older bubble plumes such as within LC convergences. Therefore, the peak radius of the bubble size distribution is a convenient way to distinguish between actively breaking waves ($a_p > 300$ μm) and LC convergences ($a_p < 200$ μm). At greater depth the size distribution is shifted toward smaller bubble radii (Figure 1b).

[6] Surprisingly, the dissipation rate drops by at least a factor 20 within the LC convergence (Figure 1c), yielding dissipation rates smaller than predicted by wall layer scaling. Enhanced dissipation rates occur briefly when a breaking wave passes the sensor, e.g., at t = 11:21.

2.2. Average LC Signal

[7] The following analysis is based on 17 well defined events when the instrument package crosses a LC convergence and no significant wave breaking occurs within the first 90s, all of them displaying the same qualitative behaviour as the event shown in Figure 1. To extract any consistent signatures, 10-minute segments of each event are conditionally sampled and averaged (Figure 2). The events are centered (t = 0) at the time when the air fraction at 2.5 m surpasses the median value at that depth, $\gamma > 5 \times 10^{-6}$. Prior to averaging, air fraction and dissipation are normalized in log-space,

$$\varepsilon_n = \log(\varepsilon/\varepsilon_{\min})/\log(\varepsilon_{\max}/\varepsilon_{\min}) \tag{1}$$

and

$$\gamma_n = \log(\gamma/\gamma_{\min})/\log(\gamma_{\max}/\gamma_{\min}), \tag{2}$$

where the maximum and minimum values are extracted from the individual 10-minute segments. Peak bubble radii a_p are normalized by a_{cr} = 150 μm, i.e. the approximate peak bubble radius separating wave breaking and LC events.

[8] Despite the variability due to the small sample size, the average signals show a strong signature of LC (Figure 2). Convergences are associated with an increase in air fraction, most noticeable at the deeper sensor. The air fraction at 0.85m is strongly affected by breaking waves and the increase of γ(0.85m) within LC convergences is less pronounced (Figure 2a). This is also seen in the peak radius of the bubble size distribution, which switches from larger bubbles $a_p/a_{cr} \geq 1$, indicative of young bubble clouds in breaking waves, to $a_p/a_{cr} \ll 1$ which exclude actively breaking waves (Figure 2b). At the lower resonator air fractions outside the convergence zone are close to the noise level of the sensor and no peak in the size distribution can be established. As air fraction increases within the bubble plume, a_p becomes better defined, resulting in an apparent

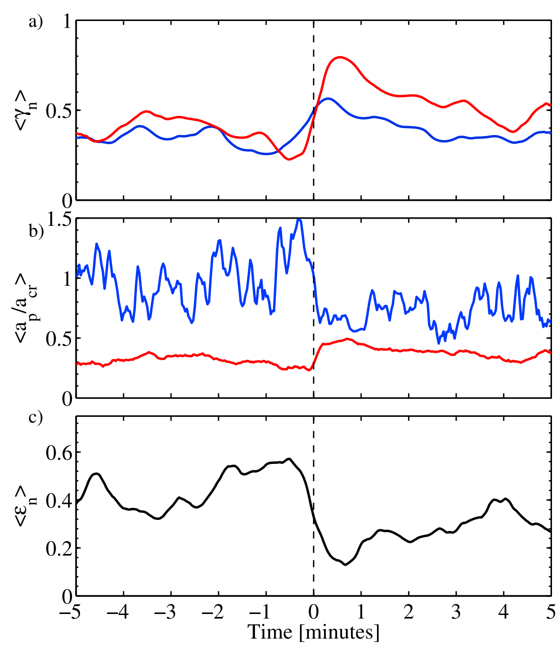

Figure 2. Average signal associated with Langmuir convergences. (a) Normalized air fraction $\log(\gamma/\gamma_{\min})/\log(\gamma_{\max}/\gamma_{\min})$ at 2.5m (red) and 0.85m (blue). (b) Normalized peak radius of bubble size distribution at 2.5m (red) and 0.85m (blue). (c) Normalized dissipation $\log(\varepsilon/\varepsilon_{\min})/\log(\varepsilon_{\max}/\varepsilon_{\min})$ at 0.8m–1.5m.

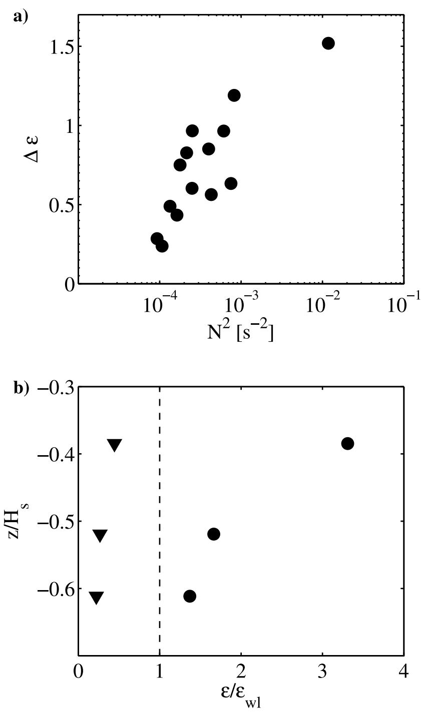

Figure 3. (a) Normalized dissipation change $\Delta\varepsilon$ as a function of bubble-induced near-surface stratification N^2. (b) Normalized dissipation depth profile within Langmuir convergences (triangle) and outside (dots).

increase in the peak radius, but still $a_p/a_{cr} \ll 1$. As the instrument drifts into the bubble plume dissipation drops significantly and remains suppressed for at least 3 minutes, on average. For each individual event a characteristic dissipation change

$$\Delta\varepsilon = \frac{\varepsilon(\tau_1) - \varepsilon(\tau_2)}{\varepsilon_{wl}} \tag{3}$$

with -45 s $< \tau_1 < -5$ s, 0 s $< \tau_2 < 40$ s is calculated. Reduction of dissipation ranges from 20% to 1.5 times the wall layer dissipation.

3. Bubble-Induced Stratification

[9] Since wave breaking is the primary cause for enhanced near-surface dissipation [*Gemmrich and Farmer*, 2004; *Gemmrich*, 2010], reduced turbulence in LC convergences could be related to a reduced wave breaking rate preferentially close to the convergence area. However, based on simultaneous video recordings, breaking rates seem not to correlate with the position relative to LC convergences. Instead, stratification effects due to gradients in the near-surface bubble-induced air fraction are likely causing the observed dissipation reduction. Void fraction measurements close to the surface, γ_s, are not available. However, the profile of acoustical backscatter from the DopBeam extends to the surface and is roughly linear, suggesting an exponential decay of air fraction [*Vagle et al.*, 2010]. Thus, the near surface air fraction γ_s is estimated from the two lower observations via linear interpolation in log-space (Figure 1a). Stratification within the Langmuir convergences can then be characterized by the near-surface buoyancy frequency N:

$$N^2 = g\frac{\partial\gamma}{\partial z} \approx g\frac{\gamma_s - \gamma_1}{z_s - z_1}, \tag{4}$$

with g gravitational acceleration, z depth, and the subscripts s, 1 refer to 0.05m and 0.85m depth, respectively.

[10] The Ozmidov scale $L_O = (\varepsilon/N^3)^{1/2}$ from individual LC events is generally less than the depth of the dissipation measurement, with an average value $\overline{L_O} = 0.68$m, and the average characteristic buoyancy time scale $\tau_B = w'/(\gamma g)$, with turbulent velocity $w' = (\varepsilon z)^{1/3}$, $\overline{\tau_B} = 35$ s is short compared to the lifetime of bubble plumes. Thus, bubble-induced buoyancy forces are relevant in this near-surface environment. Indeed, the reduction of turbulence dissipation $\Delta\varepsilon$ shows a strong correlation with the buoyancy frequency (Figure 3a). These results also indicate a minimum stratification corresponding to $N^2_{cr} \approx 5 \times 10^{-5}\mathrm{s}^{-2}$ for turbulence suppression to occur.

[11] *Smith* [1998] observed strong oscillations in the strength of LC and hypothesized that bubbles may influence the dynamics of LC. He estimated that a reduced gravity acceleration of $g' = 10^{-4}\mathrm{m\ s}^{-2}$ could stop a typical downwelling of 0.06m s^{-1} within 10 minutes. This acceleration corresponds to a near-surface stratification $N^2 = g'/(z_1 - z_s) = 1.3 \times 10^{-4}\mathrm{s}^{-2}$, which is well within the range observed here (Figure 3a).

4. Discussion

[12] In the classical wall layer flow dissipation decreases with distance from the boundary as $\varepsilon_{wl}(z) \propto |z|^{-1}$. However, in a wind-driven sea the depth dependence of ε is generally stronger and $\varepsilon(z) \propto |z|^n$, $n < -1$ (for references see, e.g., *Burchard et al.* [2008]). Our observations are within the range of wave-enhanced turbulence $|z| < H_s$. Outside LC convergences dissipation rates are up to 3 orders of magnitude larger than ε_{wl}, and show a strong depth dependence $n \approx -3$, both features being consistent with previous observations of wave-enhanced turbulence (Figure 3b). However, within LC convergences dissipation rates are significantly smaller than ε_{wl} and the depth dependence is roughly consistent with constant stress layer scaling, $n \approx -1$ (Figure 3b). On the other hand, *Thorpe et al.* [2003] found "Dissipation is enhanced in the convergence region of Langmuir circulation at depths to about 10 m" and "dissipation rates follow a law of the wall scaling", based on turbulence measurements from an AUV. However, those observations cover a depth range $1.55 \le H_s/z \le 15.9$ and are therefore below the region directly affected by wave breaking.

[13] Langmuir circulation form the largest eddies of the turbulent surface layer and thus may modulate the near-surface turbulence. Combining the results of *Thorpe et al.* [2003] with the results discussed here, following scaling of turbulence in the presence of Langmuir circulation emerges (Figure 4): i) near the surface, but outside LC convergences, wave breaking is the dominant process, resulting in enhanced dissipation rates $\varepsilon \gg \varepsilon_{wl}$, and weak buoyancy effects, $L_O \gg z$, and the turbulent time scale associated with wave breaking is much shorter than the characteristic buoyancy time scale. ii) In the near-surface region of LC convergences vertical

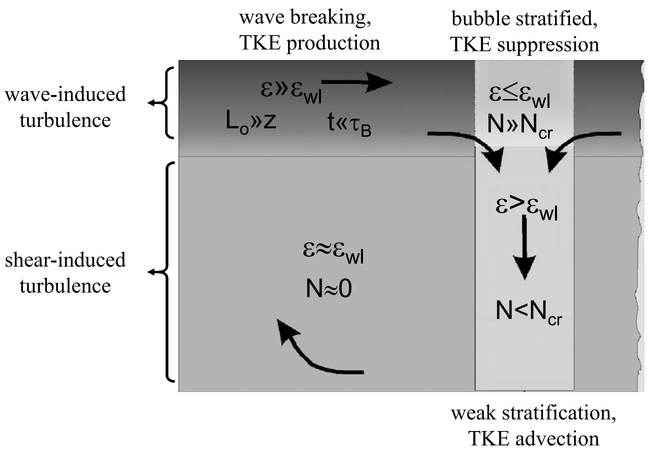

Figure 4. Schematic of bubble-induced stratification affecting turbulence levels in the near-surface layer. The vertical light gray bar represents a LC convergence zone.

gradients in air fraction are persistent and strong enough to create a stable stratification ($N > N_{cr}$), which suppresses the larger, energy containing eddies; $L_O \leq z$, and relevant time scales are comparable to the buoyancy timescale. The reduced energy at the larger end on the turbulence cascade results in significantly reduced dissipation rates $\varepsilon < \varepsilon_{wl}$. iii) Turbulence scaling in the region below the wave-enhanced layer is generally consistent with wall layer scaling. However, within the convergence zones advection of turbulence from above, but not necessarily from within the wave-enhanced layer, results in enhanced turbulence levels $\varepsilon > \varepsilon_{wl}$, but $n \approx -1$, as observed by *Thorpe et al.* [2003].

[14] This separation of the two turbulence regimes within the LC convergences will have important implications on the size distribution of bubbles and buoyant particles (like oil droplets). Depending on the location of the source of the particles two different scenarios may exist: Infrequent, energetic breakers may inject bubbles to great enough depths where vertical velocities are strong enough to keep even large bubbles in suspension, creating zones of retention [*Stommel*, 1949]. On the other hand, for sources at the surface, such as bubble generation in spilling breakers, or oil spills, those particles will accumulate near the surface within the convergence zones, rather than being drawn down. Similarly, larger bubbles cannot be kept in suspension, resulting in a truncated bubble size distribution and a less effective bubble-mediated air-sea gas exchange.

[15] **Acknowledgments.** This work evolved from a series of collaborative studies of Langmuir circulation with David Farmer. Svein Vagle provided the bubble size distributions and Andy Jessup and Jim Edson provided wave and wind stress data. Data collection was funded by the Office of Naval Research as part of the FAIRS project. Reviews by an anonymous reviewer and by J. Smith helped to improve the manuscript.

[16] The Editor thanks two anonymous reviewers for their assistance in evaluating this paper.

References

Burchard, H., et al. (2008), Observational and numerical modeling methods for quantifying coastal ocean turbulence and mixing, *Prog. Oceanogr.*, *76*(4), 399–442.

D'Asaro, E. (2001), Turbulent vertical kinetic energy in the ocean mixed layer, *J. Phys. Oceanogr.*, *31*, 3530–3537.

Deane, G. B., and M. D. Stokes (2002), Scale dependence of bubble creation mechanisms in breaking waves, *Nature*, *418*(6900), 839–844.

Farmer, D. M., and M. Li (1995), Patterns of bubble clouds organised by Langmuir circulation, *J. Phys. Oceanogr.*, *26*, 1426–1440.

Gemmrich, J. (2010), Strong turbulence in the wave crest region, *J. Phys. Oceanogr.*, *40*(3), 583–595.

Gemmrich, J. R., and D. M. Farmer (2004), Near-surface turbulence in the presence of breaking waves, *J. Phys. Oceanogr.*, *34*(5), 1067–1086.

Kukulka, T., A. J. Plueddemann, J. H. Trowbridge, and P. P. Sullivan (2009), Significance of Langmuir circulation in upper ocean mixing: Comparison of observations and simulations, *Geophys. Res. Lett.*, *36*, L10603, doi:10.1029/2009GL037620.

Li, M., C. Garrett, and E. Skyllingstad (2005), A regime diagram for classifying turbulent large eddies in the upper ocean, *Deep Sea Res., Part I*, *52*, 259–278.

McWilliams, J. C., P. P. Sullivan, and C.-H. Moeng (1997), Langmuir turbulence in the ocean, *J. Fluid Mech.*, *334*, 1–30.

Smith, J. A. (1998), Evolution of Langmuir circulation during a storm, *J. Geophys. Res.*, *103*, 12,649–12,668.

Stommel, H. (1949), Trajectories of small bodies sinking slowly through convection cells, *J. Mar. Res.*, *8*, 24–29.

Teixeira, M. A. C., and S. E. Belcher (2010), On the structure of Langmuir turbulence, *Ocean Modell.*, *31*, 105–119.

Thorpe, S. (1992), Bubble clouds and the dynamics of the upper ocean, *Q. J. R. Meteorol. Soc.*, *118*, 1–22.

Thorpe, S., T. Osborn, J. Jackson, A. Hall, and R. Lueck (2003), Measurements of turbulence in the upper-ocean mixing layer using Autosub, *J. Phys. Oceanogr.*, *33*, 122–145.

Vagle, S., C. McNeil, and N. Steiner (2010), Upper ocean bubble measurements from the NE Pacific and estimates of their role in air-sea gas transfer of the weakly soluble gases nitrogen and oxygen, *J. Geophys. Res.*, *115*, C12054, doi:10.1029/2009JC005990.

Vagle, S., J. Gemmrich, and H. Czerski (2012), Reduced upper ocean turbulence and changes to bubble size distributions during large downward heat flux events, *J. Geophys. Res.*, *117*, C00H16, doi:10.1029/2011JC007308.